Structural insights into how GTP-dependent conformational changes in a metallochaperone UreG facilitate urease maturation

Man Hon Yuen[a,1], Yu Hang Fong[a,1], Yap Shing Nim[a,1], Pak Ho Lau[a], and Kam-Bo Wong[a,2]

[a]School of Life Sciences, Centre for Protein Science and Crystallography, Partner State Key Laboratory of Agrobiotechnology, The Chinese University of Hong Kong, Hong Kong, China

Edited by Robert J. Fletterick, University of California, San Francisco School of Medicine, San Francisco, CA, and approved November 6, 2017 (received for review July 17, 2017)

The ability of metallochaperones to allosterically regulate the binding/release of metal ions and to switch protein-binding partners along the metal delivery pathway is essential to the metallation of the metalloenzymes. Urease, catalyzing the hydrolysis of urea into ammonia and carbon dioxide, contains two nickel ions bound by a carbamylated lysine in its active site. Delivery of nickel ions for urease maturation is dependent on GTP hydrolysis and is assisted by four urease accessory proteins UreE, UreF, UreG, and UreH(UreD). Here, we determined the crystal structure of the UreG dimer from *Klebsiella pneumoniae* in complex with nickel and GMPPNP, a nonhydrolyzable analog of GTP. Comparison with the structure of the GDP-bound *Helicobacter pylori* UreG (*Hp*UreG) in the $UreG_2F_2H_2$ complex reveals large conformational changes in the G2 region and residues near the $_{66}CPH_{68}$ metal-binding motif. Upon GTP binding, the side chains of Cys66 and His68 from each of the UreG protomers rotate toward each other to coordinate a nickel ion in a square-planar geometry. Mutagenesis studies on *Hp*UreG support the conformational changes induced by GTP binding as essential to dimerization of UreG, GTPase activity, in vitro urease activation, and the switching of UreG from the $UreG_2F_2H_2$ complex to form the $UreE_2G_2$ complex with the UreE dimer. The nickel-charged UreE dimer, providing the sole source of nickel, and the $UreG_2F_2H_2$ complex could activate urease in vitro in the presence of GTP. Based on our results, we propose a mechanism of how conformational changes of UreG during the GTP hydrolysis/binding cycle facilitate urease maturation.

metallochaperones | urease maturation | G protein | *Helicobacter pylori* | nickel

Nearly half of all enzymes contain metals in their active sites (1, 2). Cells have evolved mechanisms to maintain metal homeostasis and to ensure metalloenzymes receive the correct metal ions (3, 4). Metals at the top of the Irving–Williams series such as nickel, copper, and zinc, can form more stable protein–metal complexes than weaker metals such as magnesium and can inactivate enzymes that require the less competitive metals to function (5, 6). Therefore, the free cytoplasmic concentrations of these competitive metal ions are tightly controlled and are kept at subnanomolar concentrations to avoid cytotoxicity (5, 7). One strategy of delivering the correct metal to a metalloenzyme is through specific protein–protein interactions with metallochaperones (4). Typically, metal ions are passed from one metallochaperone to another before they are eventually inserted into the catalytic site of metalloenzymes (8–10). Conceptually, this scheme requires the ability of metallochaperones to allosterically regulate the binding/release of metal ions and to change protein-binding partners along the metal delivery pathway.

Urease, catalyzing the hydrolysis of urea into ammonia and carbon dioxide, contains two nickel ions bound by a carbamylated lysine residue in its active site (11). The enzyme is a virulence factor for *Helicobactor pylori* because the pathogen uses the neutralizing ammonia released for its survival in acidic stomach (12). Delivery of nickel and urease maturation are assisted by four urease accessory proteins, namely, UreE, UreF, UreG, and UreH (or UreD in other species) (13–17). The urease maturation is dependent on GTP hydrolysis and involves the formation of an activation complex containing UreF, UreG, UreH, and apourease (13, 18–23). UreF can form a $UreF_2H_2$ complex with UreH in a 2:2 stoichiometry (24). The formation of the $UreF_2H_2$ complex is essential to the recruitment of UreG to form the $UreG_2F_2H_2$ complex (20, 24, 25). UreG belongs to the G3E family of SIMIBI (signal recognition particle, MinD, and BioD) class GTPases (26, 27), and undergoes a GTP-dependent dimerization upon binding of nickel (20). We have previously shown that the Ni/GTP-bound UreG dimer, providing the sole source of nickel, can activate urease in vitro in the presence of the $UreF_2H_2$ complex (20), which can induce conformational changes in apourease that are essential for nickel delivery (13, 28). It has been shown recently that nickel can be transferred from another metallochaperone UreE to UreG by forming a $UreE_2G_2$ complex (29). In this study, we determined the crystal structure of *Klebsiella pneumoniae* UreG in complex with nickel and Guanylyl imidodiphosphate (GMPPNP). Together with our biochemical and mutagenesis studies, we have demonstrated how conformational changes induced by the GTP hydrolysis/binding cycle in the metallochaprone UreG facilitate urease maturation by modulating its binding to the nickel ion and protein-binding partners.

Significance

Our work provides insights into how cells solve the problem of delivering nickel, a toxic metal, to the active site of a metalloenzyme such as urease. Urease, a nickel-containing enzyme, is a virulence factor for *Helicobacter pylori*, which infects half of the human population and causes peptic ulcers. Supported by structural and biochemical evidence, we present a paradigm on how a metallochaperone UreG couples GTP hydrolysis/binding to allosterically control the binding/release of nickel ions and to switch protein-binding partners along the metal-delivery pathway so that the nickel ions are passing from one metallochaperone to another, without releasing the "free" toxic metal to the cytoplasm.

Author contributions: M.H.Y., Y.H.F., Y.S.N., and K.-B.W. designed research; M.H.Y., Y.H.F., Y.S.N., P.H.L., and K.-B.W. performed research; M.H.Y., Y.H.F., Y.S.N., and K.-B.W. analyzed data; and M.H.Y. and K.-B.W. wrote the paper.

The authors declare no conflict of interest.

This article is a PNAS Direct Submission.

Data deposition: The atomic coordinates and structure factors have been deposited in the Protein Data Bank, www.wwpdb.org (PDB ID code 5XKT).

[1]M.H.Y., Y.H.F., and Y.S.N. contributed equally to this work.

[2]To whom correspondence should be addressed. Email: kbwong@cuhk.edu.hk.

This article contains supporting information online at www.pnas.org/lookup/suppl/doi:10.1073/pnas.1712658114/-/DCSupplemental.

Result

Crystal Structure of *Kp*UreG in Complex with Nickel and GMPPNP. We have previously determined the structure of *H. pylori* GDP-bound UreG (*Hp*UreG) in the $UreG_2F_2H_2$ complex (20). To understand the conformational changes of UreG upon binding of nickel and GTP, we determined the crystal structure of UreG from *K. pneumoniae* (*Kp*UreG) in complex with GMPPNP and nickel to a resolution of 1.8 Å (*SI Appendix*, Table S1 and Fig. 1*A*, PDB ID code 5XKT). To improve the quality of crystals, a truncated *Kp*UreG(ΔN4ΔC1) was used for structure determination. *Kp*UreG, sharing 64% sequence identity with *Hp*UreG, is six residues longer (Fig. 1*C*). To avoid confusion, we will use the sequence numbering of *Hp*UreG in subsequent structural comparison.

*Kp*UreG adopts a SIMIBI-like fold with a seven-stranded β-sheet sandwiched by 10 α-helices, and exists as a dimer in the crystal structure. The invariant CPH metal binding motif from each protomer of *Kp*UreG is juxtaposed to bind a nickel ion, which is coordinated by Cys66 and His68 in a square-planar geometry (*SI Appendix*, Fig. S1 *A* and *C*). *Kp*UreG contains the canonical G1–G5 motifs for guanine nucleotide recognition (Fig. 1 *B* and *C*). One molecule of GMPPNP was bound to each of the two *Kp*UreG protomers at the dimerization interface, forming extensive hydrogen bonds with residues of the G1–G5 motifs (Fig. 1*B* and *SI Appendix*, Fig. S1*D*). Phosphate groups of GMPPNP are wrapped around by G1 residues that constituted the P loop. The guanine base is sandwiched between the aliphatic side chains of Lys146 and Lys179, forming canonical hydrogen bonds to Asp148 of the G4 motif and to backbone amides of the G5 motif (Fig. 1*B*). Anomalous difference electron density maps revealed that a nickel ion occupies the magnesium-binding site in each of the nucleotide-binding pockets (*SI Appendix*, Fig. S1*B*). Noteworthy, the nickel ion is coordinated in an octahedral geometry, which is commonly observed for magnesium ion in GTPases (30, 31). Presumably, the nickel ions, being a more competitive ion, displaced the active site magnesium ions in the crystallization conditions used. Our result suggests that while nickel ion is required for the formation of the nickel-charged UreG dimer, excess nickel ions should be inhibitory because they could displace the magnesium ions in the active sites.

GTP Binding Induces Large Conformational Changes in UreG. To understand the GTP-induced conformational changes, the structure of Ni/GMPPNP-bound *Kp*UreG was compared with the crystal structure of GDP-bound *Hp*UreG in complex with $UreF_2H_2$ (20). Most residues of the Ni/GMPPNP-bound *Kp*UreG were superimposable with the GDP-bound *Hp*UreG (Fig. 2 *A* and *B*), suggesting that the two proteins are structurally homologous with each other. Notably, large conformational changes were observed in the G2 region (β2 and α2; residues 37–52) and in residues near the CPH nickel-binding motif (residues 62–68) (Fig. 2*B* and Movie S1).

Taking a closer look at the nucleotide-binding pocket reveals that the invariant residue Asp37 (or Asp43 in *Kp*UreG) plays an instrumental role in initiating the GTP-dependent conformational changes. Upon GTP binding, charge–charge repulsion between the γ-phosphate and Asp37 pushes the invariant residue away from the nucleotide-binding pocket (Fig. 2*C*), causing Asp37 and Ile38 to form backbone hydrogen bonds with Val61, Thr63, and Gly64. As a result, β2 and β3 of Ni/GMPPNP-bound *Kp*UreG is extended (Fig. 2*C*). This "zip-up" motion of β2 and β3 strands propagates the conformational changes to the CPH metal-binding motif, which is located at the end of β3. The Cys66 and His68 of each protomer move in an opposite direction toward the metal binding site and coordinate a nickel ion at the dimer interface. Asp102 of the G3 motif moves toward the CPH motif and forms hydrogen bonds to Asn103 and His68, stabilizing the square-planar coordination geometry of the CPH motif (*SI Appendix*, Fig. S2*A*). At the same time, GTP binding causes helix-2 to tilt by ∼35° toward the nucleotide-binding site, bringing Glu42 to form a salt bridge with Arg130 of the opposite protomer (*SI Appendix*, Fig. S2*B*). In addition, the opposite protomer of UreG undergoes a rigid-body movement toward the bound nucleotide so that Tyr152 and Val153 of the opposite protomer form two extra hydrogen bonds to the guanine ring of GMPPNP (*SI Appendix*, Fig. S2*C*).

We have previously shown that addition of nickel ions and GTP can dissociate UreG from the $UreG_2F_2H_2$ complex (20). The crystal structure of Ni/GMPPNP-bound *Kp*UreG determined here explains how the conformational changes of UreG induce the dissociation. As shown in Fig. 2 *C* and *D*, the zip-up motion of β2 and β3 causes Tyr39 of the G2 motif to protrude into the $UreF_2H_2$-binding site, introducing steric clashes that break the interaction between UreG and the $UreF_2H_2$ complex.

Double Mutation D37A/E42A Abolishes the Formation of the Nickel-Charged *Hp*UreG Dimer, GTPase Activity, and in Vitro Activation of Urease. As discussed above, a structural comparison suggests that charge–charge repulsion between Asp37 and the γ-phosphate group of GTP is important in initiating the GTP-dependent conformational changes that bring Glu42 to form a salt bridge with Arg130 with the opposite protomer (*SI Appendix*, Fig. S2*B*). We argued that these residues are important in inducing the conformational changes of UreG from a GDP-bound state to a GTP-bound state. To test this hypothesis, we created a double mutant, D37A/E42A, of *Hp*UreG and tested its ability to dimerize upon addition of nickel ions and GTP. It is expected that the double mutant should favor the GDP-bound state conformation even in the presence of GTP or its analog. Circular dichroism spectra of the D37A/E42A mutant, collected at 25–42 °C, were similar to those of the wild-type *Hp*UreG, suggesting that the mutant was folded and stable at these temperatures (*SI Appendix*, Fig. S9). Based on the size-exclusion chromatography/static light-scattering (SEC/SLS) experiments, we showed that the elution profile of the D37A/E42A mutant in the presence of GTPγS was similar to that of wild-type *Hp*UreG in the presence of GDP, suggesting that the double mutant failed to undergo GTP-dependent dimerization of *Hp*UreG (Fig. 3*A*). We further showed that D37A/E42A *Hp*UreG abolished its in vitro GTPase activity (Fig. 3*B*) and its ability to activate urease in vitro (Fig. 3*C*). Taken together, our results are consistent with the conclusion that Asp37 and Glu42 are essential for the GTP-induced conformational changes that lead to UreG dimerization, which is in turn important for GTPase activity and urease activation.

D37A/E42A Double Mutation Greatly Reduces the GTP-Dependent Dissociation of *Hp*UreG from $UreG_2F_2H_2$ and the Formation of the $UreE_2G_2$ Complex. Next, we tested whether Asp37 and Glu42 are essential for the dissociation of *Hp*UreG from the $UreG_2F_2H_2$ complex. We added GDP or GTPγS to the $UreG_2F_2H_2$ complex in a buffer containing nickel (*SI Appendix*, Fig. S3). In the presence of GDP, both wild-type and D37A/E42A *Hp*UreG were able to form the $UreG_2F_2H_2$ complex. Upon addition of GTPγS, the majority of wild-type *Hp*UreG dissociated from the $UreG_2F_2H_2$ complex to form the UreG dimer (*SI Appendix*, Fig. S3). In contrast, the dissociation of UreG was greatly reduced in the D37A/E42A mutant.

In a previous study, UreG was shown to interact with UreE to form a $UreE_2G_2$ complex in the presence of GTP, but to form a $UreE_2G$ complex in the presence of GDP (29). We hypothesized that the conformational changes induced upon GTP binding will cause UreG to prefer a 2:2 stoichiometry in forming a complex with UreE. Therefore, we tested whether the D37A/E42A mutations will affect the formation of the $UreE_2G_2$ complex. *H. pylori* UreG and UreE were added in equal molar ratio in a buffer containing nickel and GDP/GTPγS (*SI Appendix*, Fig. S4).

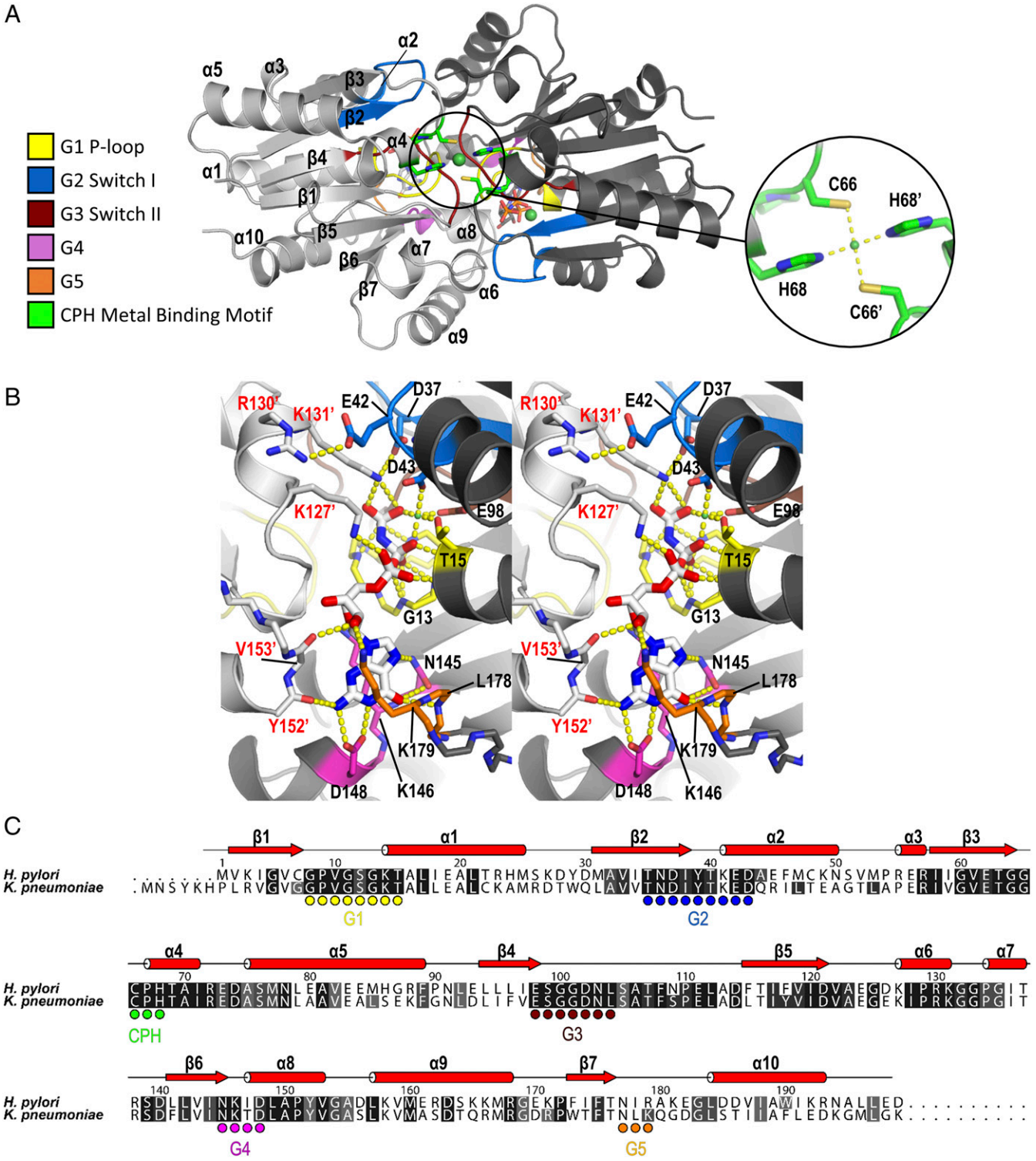

Fig. 1. Crystal structure of *Kp*UreG in complex with GMPPNP and nickel. (*A*) The structure of *Kp*UreG (PDB ID code 5XKT) was solved as a dimer in complex with GMPPNP and nickel at a resolution of 1.8 Å. Cys66 and His68 from each of the two UreG protomers (colored in light and dark gray) coordinate a nickel ion in a square-planer geometry. Conserved motif (G1–G5) and CPH metal binding motif are colored as indicated. (*B*) A stereodiagram showing the interaction between *Kp*UreG and GMPPNP. GMPPNP is sandwiched between the two *Kp*UreG protomers and forms a network of hydrogen bonds (yellow dotted lines) with residues of the G1–G5 motifs. (*C*) Sequence alignment of *Kp*UreG and *Hp*UreG. The G1–G5 and the CPH metal-binding motifs are indicated as circles. Residues are numbered according to the *Hp*UreG sequence. Apostrophes denote residues from the opposite protomer.

In the presence of GDP, both wild-type and D37A/E42A *Hp*UreG mainly formed a 2:1 complex with UreE (*SI Appendix*, Fig. S4, cyan lines). Consistent with previous findings, wild-type *Hp*UreG was able to form complex with UreE in a 2:2 stoichiometry in the presence of GTPγS (*SI Appendix*, Fig. S4, red lines). In the case of the D37A/E42A mutant, the GTP-dependent

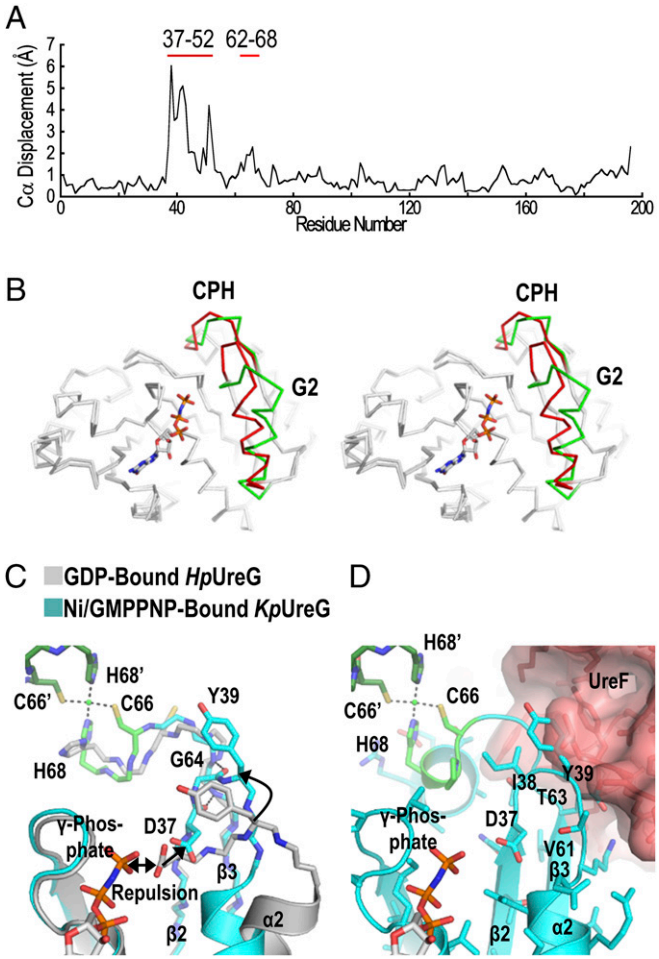

Fig. 2. Conformational changes of UreG upon GTP binding. (*A*) The structures of the GDP-bound *Hp*UreG (4HI0, chain F) and the Ni/GMPPNP-bound *Kp*UreG (5XKT, chain A) were superimposed and values of Cα displacement were plotted. (*B*) Stereodiagram highlighting significant conformational changes found in the G2 region (residues 37–52) and near the CPH metal-binding motif (residues 62–68), which are colored in green and red for the GDP-bound *Hp*UreG and the Ni/GMPPNP-bound *Kp*UreG, respectively. (*C*) Charge–charge repulsion between Asp37 and the γ-phosphate group elicits conformational changes that are propagated to the CPH metal-binding site. The repulsion pushes the Asp37 away from the nucleotide-binding site so that Asp37 and Ile38 (β2 strand) form backbone hydrogen bonds with Val61, Thr63, and Gly64 (β3 strand). This zip-up motion of the β2 and β3 strands propagates conformational changes to the CPH metal-binding motif and causes helix-2 to tilt by ∼35° toward the nucleotide-binding site. (*D*) Moreover, Tyr39 of the G2 region moves toward the $UreF_2H_2$-binding site, introducing steric clashes that promote dissociation of UreG from the $UreG_2F_2H_2$ complex. Residues from the opposite protomer are indicated by apostrophes.

formation of the $UreE_2G_2$ complex was greatly reduced. Taken together, our results suggest that the double mutation, D37A/E42A, prevents the GTP-dependent conformational changes of UreG that are essential for the dissociation of UreG from the $UreG_2F_2H_2$ complex and the formation of $UreE_2G_2$ complex.

***Hp*UreG Swaps Protein-Binding Partners During the GTP Hydrolysis/Binding Cycle.** Our structural studies suggest that UreG exists in two distinct conformational states: the GDP-bound and the GTP-bound state. UreG prefers to form the $UreG_2F_2H_2$ complex with UreF and UreH in the presence of GDP (20) (*SI Appendix*, Fig. S3), but prefers to form the $UreE_2G_2$ complex with UreE in the presence of GTPγS (29) (*SI Appendix*, Fig. S4). These observations suggest that GTP hydrolysis should change the conformational state of UreG and cause it to change protein-binding partners. To test this hypothesis, we first prepared a $UreE_2G_2$ complex by mixing nickel-charged *H. pylori* UreE dimer ($UreE_2$/Ni) with *Hp*UreG in the presence of GTP (*SI Appendix*, Fig. S5). Upon activation of GTP hydrolysis by addition of $KHCO_3$, the $UreE_2G_2$ complex was dissociated into $UreE_2G$ and a monomeric *Hp*UreG (*SI Appendix*, Fig. S6). When the $UreE_2G_2$ complex was mixed with the $UreF_2H_2$ complex, *Hp*UreG was displaced from $UreE_2G_2$ and formed the $UreG_2F_2H_2$ complex upon addition of $KHCO_3$ (Fig. 4*A*).

Next, we tested whether the $UreE_2G_2$ complex can be regenerated from the $UreG_2F_2H_2$ complex by addition of GTPγS. We prepared a *H. pylori* GDP-bound $UreG_2F_2H_2$ complex and mixed it with the nickel-charged UreE dimer (Fig. 4*B*). We showed that the majority of the $UreG_2F_2H_2$ complex remained intact despite the fact that small amounts of *Hp*UreG were dissociated from the $UreG_2F_2H_2$ complex to form the $UreE_2G$ complex (Fig. 4*B*, *Left*). This observation suggests that UreG prefers to form a complex with $UreF_2H_2$ over $UreE_2$ in its GDP-bound conformation. In contrast, addition of GTPγS to the $UreG_2F_2H_2$ complex and the nickel-charged UreE dimer resulted in the formation of the $UreF_2H_2$ and $UreE_2G_2$ complexes (Fig. 4*B*, *Right*). We further showed that *Hp*UreG could also switch from the $UreG_2F_2H_2$ complex to the $UreE_2G_2$ complex in the absence of nickel ion (*SI Appendix*, Fig. S7), suggesting that the swapping of protein-binding partners is only dependent on GTP but not on nickel. Noteworthy, the ability of *Hp*UreG to swap protein-binding partners was greatly reduced by the D37A/E42A mutations (Fig. 4*B*, *Right*), which presumably favors the GDP-bound state of UreG. Taken together, our results are consistent with the conclusion that the conformational changes upon GTP hydrolysis/binding dictate the protein-binding partners of UreG (Fig. 4*C*).

In Vitro Urease Activation Assay Suggests That UreE Is the Nickel Source for Urease Maturation. We have established an in vitro urease activation assay, in which purified samples of urease accessory proteins are added to the apourease to test how they affect *H. pylori* urease activation (20). We showed that purified nickel-charged UreG dimers ($UreG_2$/Ni), which provide the sole source of nickel, can activate urease in vitro in the presence of the $UreF_2H_2$ complex (20). It has been shown that nickel ions can be transferred from UreE to UreG via the formation of the $UreE_2G_2$ complex (29), suggesting that UreE should be the source of nickel for urease activation. To test this hypothesis, we added a purified sample of nickel-charged *H. pylori* UreE dimer ($UreE_2$/Ni) to the $UreG_2F_2H_2$ complex and apourease and showed that the urease was activated in the presence of GTP, but not in the presence of GTPγS (Fig. 5*A*). The activation was nickel dependent because adding apo-$UreE_2$ without the bound nickel ($UreE_2$) failed to activate urease (Fig. 5*A*). Moreover, the activation requires *Hp*UreG because the nickel-charged UreE dimer was not able to activate urease in the presence of the $UreF_2H_2$ complex (Fig. 5*A*).

Our results also suggest that UreG switches from the $UreG_2F_2H_2$ complex to the $UreE_2G_2$ complex upon GTP binding (Fig. 4*B* and *SI Appendix*, Fig. S7). So, we hypothesized that the resulting $UreE_2G_2$ and $UreF_2H_2$ complexes are essential to urease activation. To test this hypothesis, the nickel-charged *H. pylori* $UreE_2G_2$ and $UreF_2H_2$ complexes were added to the apourease (Fig. 5*B*). Our results showed the nickel-charged $UreE_2G_2$ complex ($UreE_2G_2$/Ni) was able to activate urease in the presence of $UreF_2H_2$ (Fig. 5*B*). The activation was nickel dependent because the $UreE_2G_2$ complex without the bound nickel failed to activate urease (Fig. 5*B*). The activity of the urease activated by $UreE_2G_2$/Ni was similar to that activated by $UreG_2$/Ni (Fig. 5*C*). Taken together, our results suggest that the nickel-charged UreE

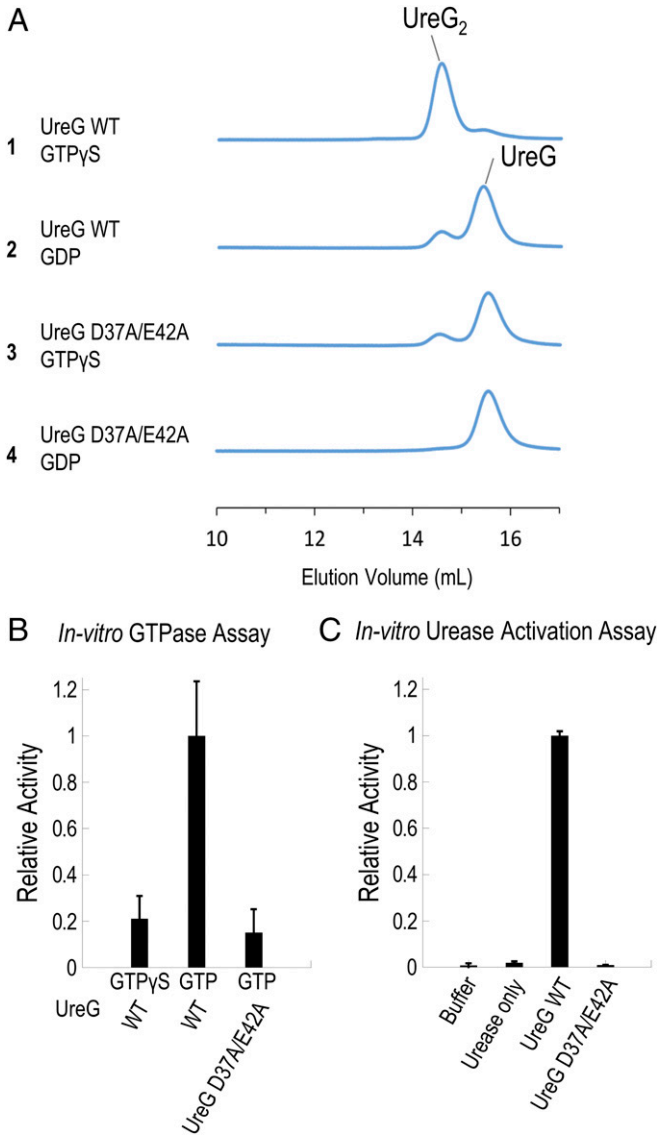

Fig. 3. Double mutation D37A/E42A abolishes the formation of the nickel-charged *Hp*UreG dimer, GTPase activity, and urease activation. (*A*) Protein samples of 30 μM *H. pylori* UreG (WT or mutant) were mixed with 45 μM nickel ion and 300 μM GTPγS/GDP and were analyzed using SEC/SLS. The wild-type UreG mainly existed as a dimer in the presence of GTPγS (injection 1), but as a monomer in the presence of GDP (injection 2). In contrast, the D37A/E42A mutant mainly existed as a monomer regardless of addition of GTPγS or GDP (injections 3 and 4). (*B*) GTP hydrolysis was followed by the amount of phosphate released using the malachite green assay as described in *Materials and Methods*. A total of 5 μM of UreG (WT or D37A/E42A mutant) was incubated with 300 μM of GTP/GTPγS in 2 mM $MgSO_4$, 10 mM potassium bicarbonate, 4 μM $NiSO_4$, 200 mM NaCl, 1 mM TCEP, 20 mM Hepes pH 7.5 buffer at 37 °C for 60 min. The hydrolysis rates were determined and analyzed by linear regression using the PRISM program (GraphPad Software). The hydrolysis rate of the wild-type *Hp*UreG was significantly different from those of the double mutant and the GTPγS control ($P < 0.01$), while there were no significant differences between the mutant and the GTPγS control. Moreover, the slope of the regression lines for the double mutant and the GTPγS were not significantly deviated from zero. Relative activity was normalized using the hydrolysis rate of wild-type *Hp*UreG (43 ± 7 nM phosphate/μM UreG/min). (*C*) A total of 10 μM apourease was activated by 40 μM UreG (WT or mutant) and 20 μM $UreF_2H_2$ complex in 2 mM $MgSO_4$, 10 mM potassium bicarbonate, 45 μM $NiSO_4$, 300 μM GTP, and 20 mM Hepes pH 7.5, 200 mM NaCl, 1 mM TCEP, at 37 °C for 20 min. Urease activity was determined by measuring the amount of ammonia released. In the "urease only" control, no urease accessory protein was added, while in the "buffer" control, no apourease or urease accessory proteins were added. Relative activity was normalized using the activity of urease activated by wild-type *Hp*UreG (304 ± 5 μmol NH_3/mg urease/min).

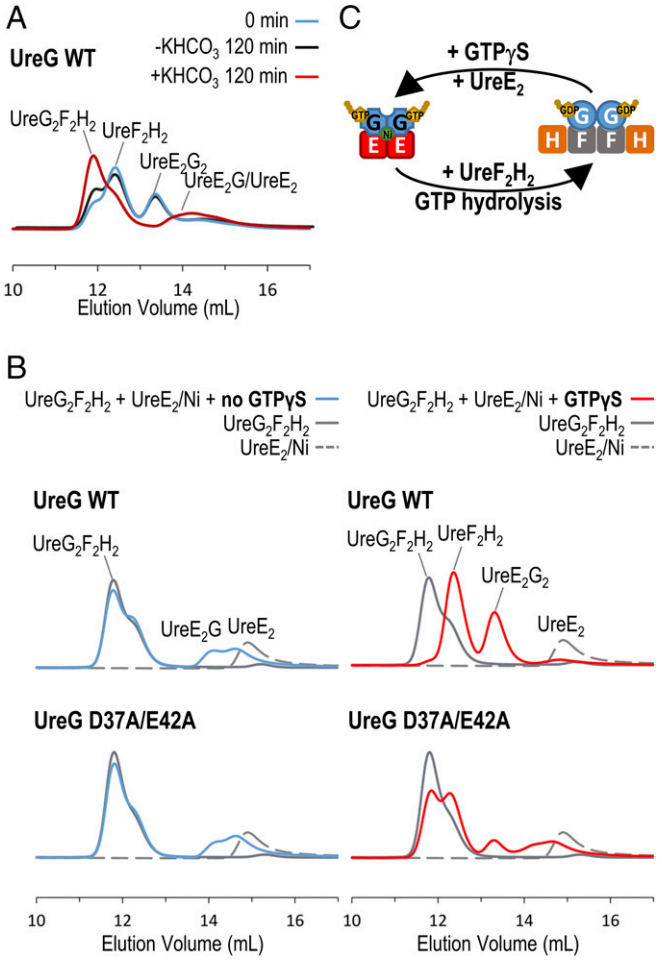

Fig. 4. UreG swaps protein-binding partners during the GTP hydrolysis/binding cycle. (*A*) Equal molar ratio (15 μM) mixture of *H. pylori* $UreE_2G_2$/Ni and $UreF_2H_2$ complexes (cyan) was incubated in 2 mM $MgSO_4$, 1 mM GTP, 0.2 mM TCEP, 100 mM NaCl, 20 mM Hepes, pH 7.2 with (red) or without (black) 10 mM $KHCO_3$ at 37 °C for 120 min. The protein samples were then analyzed by SEC/SLS. Upon activation of GTP hydrolysis by $KHCO_3$ (red), the $UreE_2G_2$ complex disappeared and the majority of the $UreF_2H_2$ complex was converted to the $UreG_2F_2H_2$ complex. (*B*) A total of 15 μM $UreG_2F_2H_2$ complex (gray solid lines) and 15 μM $UreE_2$/Ni dimer (gray dotted lines) was added to 2 mM $MgSO_4$, 0.2 mM TCEP, 100 mM NaCl, 20 mM Hepes, pH 7.2 buffer with (red lines) or without (cyan lines) 300 μM GTPγS. The protein samples were analyzed by SEC/SLS. In the absence of GTPγS (*Left*), only a small amount of UreG dissociated from the $UreG_2F_2H_2$ complex to form the $UreE_2G$ complex. In the presence of GTPγS (*Right*), wild-type UreG completely dissociated from the $UreG_2F_2H_2$ complex to form the $UreE_2G_2$ complex with the UreE dimer. For the UreG D37A/E42A mutant, the GTP-dependent swapping of protein-binding partners was greatly abolished. (*C*) Our results suggest that the preference of protein-binding partners is dictated by conformational changes in UreG induced by GTP binding/hydrolysis.

dimer, providing the sole source of nickel, can activate urease via the formation of the nickel-charged $UreE_2G_2$ complex.

To show that protein–protein interactions are essential to urease activation, we set up the protein components of the in vitro urease activation assay in either side of a dialysis membrane in a two-chamber dialyzer as indicated in *SI Appendix*, Fig. S10. The dialysis membrane allows diffusion of nickel ions but prevents direct protein–protein interactions across the membrane. Consistent with what was observed in Fig. 5*A*, urease was activated when $UreE_2$/Ni, providing the sole source of nickel ions, was added to the chamber on the right where $UreG_2F_2H_2$ and

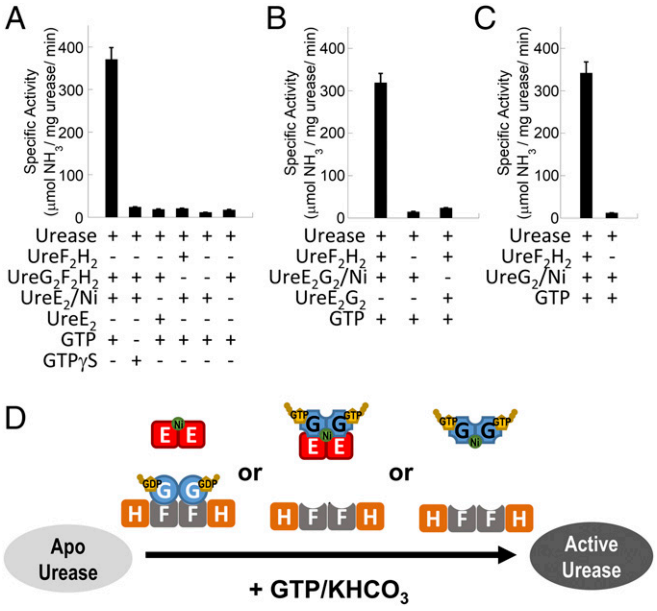

Fig. 5. In vitro urease activation assays suggest that nickel-charged UreE dimer provides the nickel source for urease maturation. The in vitro urease activation assay was performed by incubating 10 μM *H. pylori* apourease with 20 μM of *H. pylori* urease accessory proteins/complexes as indicated at 37 °C for 20 min in 20 mM Hepes pH 7.5 buffer containing 1 mM GTP or GTPγS, 2 mM $MgSO_4$, 10 mM potassium bicarbonate, 200 mM NaCl, and 1 mM TCEP. Urease activity was measured by the amount of ammonia released. Protein samples of urease accessory proteins/complexes were prepared and analyzed by SEC/SLS (*SI Appendix*, Fig. S8). Nickel-charged UreE dimer ($UreE_2$/Ni) and nickel-charged $UreE_2G_2$ ($UreE_2G_2$/Ni) complex were prepared and analyzed by atomic absorption spectroscopy (*SI Appendix*, Fig. S5). (*A*) Apourease was activated only when 20 μM nickel-charged UreE dimer, providing the sole source of nickel, was added with the presence of 20 μM $UreG_2F_2H_2$ complex. (*B*) Apourease was activated when 20 μM nickel-charged $UreE_2G_2$ complex ($UreE_2G_2$/Ni), providing the sole source of nickel, was added with the presence of 20 μM $UreF_2H_2$ complex. (*C*) Apourease (10 μM) was activated when 20 μM nickel-charged UreG dimer ($UreG_2$/Ni), providing the sole source of nickel, was added with the presence of 20 μM $UreF_2H_2$ complex. (*D*) Schematic diagram summarizing the combination of urease accessory proteins/complexes that can activate urease in the in vitro assay. Either $UreE_2$/Ni, $UreE_2G_2$/Ni, or $UreG_2$/Ni can provide the nickel source for urease activation.

apourease were present (*SI Appendix*, Fig. S10, A1). On the other hand, urease activation was greatly abolished when $UreE_2$/Ni was separated from $UreG_2F_2H_2$ and apourease by the dialysis membrane (*SI Appendix*, Fig. S10, A2), suggesting that the interactions of $UreE_2$/Ni with other proteins in the system are essential to urease activation. Moreover, our results do not support the alternative hypothesis that nickel ions are released from $UreE_2$/Ni into the solution, and then, through diffusion, picked up by UreG for urease activation. As a control, we showed that free nickel ions, if present, in the left chamber could diffuse across the dialysis membrane and activate urease in the right chamber with $UreG_2F_2H_2$ (*SI Appendix*, Fig. S10, C1). While addition of Ni/GTP induces the dissociation of $UreG_2F_2H_2$ into $UreG_2$/Ni and $UreF_2H_2$ that could activate urease in vitro (20), it is unlikely to be physiologically relevant because cytoplasmic free nickel ions are kept at subnanomolar concentrations to avoid cytotoxicity (5, 7). Interestingly, urease activation was inhibited when apo-$UreE_2$ was added to the left chamber (*SI Appendix*, Fig. S10, C2), presumably due to the removal of free nickel ions from the solution. Taken together, our results reinforce the suggestion that the delivery of nickel ions for urease activation requires interactions of $UreE_2$/Ni with other urease accessory proteins.

Similarly, urease was activated when $UreG_2$/Ni, providing the sole source of nickel ions, was added to the right chamber where $UreF_2H_2$ and apourease were present (*SI Appendix*, Fig. S10, B1), but not when $UreG_2$/Ni was added to the left chamber (*SI Appendix*, Fig. S10, B2). These observations suggest that interactions between $UreG_2$/Ni and $UreF_2H_2$/apourease are essential to urease activation. Moreover, addition of free nickel ions failed to activate the urease in the absence of UreG (*SI Appendix*, Fig. S10, C3), suggesting that UreG is required for the activation.

Discussion

In this study, we determined the crystal structure of the *Kp*UreG dimer in complex with nickel ions and a nonhydrolyzable analog of GTP, GMPPNP. We showed that UreG exists in two distinct conformational states: the GTP-bound state and the GDP-bound state. Structural comparison reveals that GTP binding induces conformational changes in the G2 region, which are propagated to the CPH nickel-binding motif. The main theme of this study was to understand how conformational changes of UreG play essential roles in urease maturation.

First, our work provides structural insights into why GTP-dependent conformational changes would induce nickel binding and why GTP hydrolysis would promote nickel release that is essential for urease maturation. In the crystal structure of the *H. pylori* GDP-bound UreG in the $UreG_2F_2H_2$ complex (20), Cys66 and His68 are pointing away from each other and are not in a position to chelate a nickel ion (*SI Appendix*, Fig. S2*A*). Upon GTP binding, Cys66 and His68 from both protomers of UreG form a square-planar coordination that chelates a nickel ion at the dimeric interface (Fig. 1*A* and *SI Appendix*, Fig. S2). Since the square-planar coordination is preferred for Ni^{2+} (for having a d^8 electron configuration) but not for other ions such as Zn^{2+} (31), it justifies the observation that UreG has a stronger affinity toward Ni^{2+} than Zn^{2+} in the presence of GTP (20, 29). GTP hydrolysis reverts UreG to the GDP-bound conformational state and promotes nickel release.

Second, we showed that the conformational state of UreG dictates the formation of different protein complexes that are involved in urease maturation. It has been shown that *Hp*UreG dissociates from the $UreG_2F_2H_2$ complex in the presence of nickel ions and GTPγS (20). Here we showed that binding of GTP induces conformational changes in the G2 region so that the invariant residue Tyr39 of UreG makes steric clashes with UreF (Fig. 2*D*), facilitating the dissociation of UreG from the $UreG_2F_2H_2$ complex. Interestingly, we showed that the UreE dimer can take the UreG from the $UreG_2F_2H_2$ complex in the presence of GTPγS (Fig. 4*B* and *SI Appendix*, Fig. S7) to form the $UreE_2G_2$ complex.

That conformational changes are essential for UreG to change protein partners is further supported by mutagenesis studies. We identified that the invariant residues Asp37 and Glu42 play important roles in the conformational changes upon GTP binding. In the GDP-bound state of UreG, Asp37 partially occupies the γ-phosphate–binding pocket (Fig. 2*C*). Binding of GTP creates charge–charge repulsion between the γ-phosphate group of GTP and Asp37, which induces large conformational changes in the G2 region (Fig. 2). Notably, helix-2 turns ∼35° toward the nucleotide-binding site, bringing Glu42 to form an intermolecular salt bridge with another invariant residue, Arg130, that stabilizes the formation of the UreG dimer. The D37A/E42A mutations greatly abolished GTP-dependent dimerization of UreG and prevented dissociation of UreG from the $UreG_2F_2H_2$ complex to form the $UreE_2G_2$ complex (Figs. 3 and 4). Apparently, the double mutation of D37A/E42A locks the conformation of UreG in the GDP-bound state even in the presence of GTP.

We have previously shown that the nickel-charged UreG dimer can activate urease in vitro, likely via the formation of an activation complex with $UreF_2H_2$ and urease (13, 19, 20, 24).

It has been suggested that the nickel-charged UreG dimer gets its nickel from UreE. Yang and coworkers have demonstrated that UreE can receive its nickel from HypA and can form a $UreE_2G_2$ complex with UreG in the presence of GTP (29, 32, 33). Mutagenesis (29) and modeling (34) studies suggest that the metal binding sites of UreE and UreG should face toward each other and the nickel ion can be transferred from UreE to UreG within the $UreE_2G_2$ complex (29). Here, we provided direct evidence that the nickel-charged UreE dimer is the source of nickel, for it can activate urease in the presence of $UreG_2F_2H_2$ and GTP (Fig. 5*A*). Our results also show that the nickel-charged $UreE_2G_2$ complex, which provides the sole source of nickel in the in vitro assay, can activate urease in the presence of $UreF_2H_2$ (Fig. 5*B*).

Taken together, the ability of UreG to form different protein complexes during the GTP hydrolysis/binding cycle provides a mechanism of how GTP-dependent conformational changes in UreG facilitate urease maturation (Fig. 6 and Movie S1). GTP binding induces conformational changes in UreG, causing it to dissociate from the $UreG_2F_2H_2$ complex and to form the $UreE_2G_2$ complex with the nickel-charged UreE dimer (Fig. 6). Moreover, the dissociation of the $UreG_2F_2H_2$ complex also yields the $UreF_2H_2$ complex, which can form a complex with the apourease (18, 35) making it ready for activation by either $UreG_2$/Ni or $UreE_2G_2$/Ni (Fig. 5 *B* and *C*). GTP hydrolysis reverts UreG to its GDP-bound state, disrupting the square-planar coordination by Cys66/His68 and promoting release of nickel ion. It is unclear how the nickel ion released from UreG eventually reaches the catalytic site of urease. Recently, it has been suggested that the nickel ion may pass to UreF, and then go through a tunnel of UreH to the urease (36–38). After GTP hydrolysis-dependent activation of urease, the GDP-bound $UreG_2F_2H_2$ is regenerated (Fig. 4*A*), which is ready for the next round of urease activation (Fig. 6).

It is unclear whether the $UreE_2G_2$ complex can directly activate urease by forming a bigger activation complex with $UreF_2H_2$ and apourease or whether the activation requires the dissociation of the nickel-charged UreG dimer from the $UreE_2G_2$ complex. It has been suggested that the UreG–UreE interaction involves the protein surfaces near the nickel binding site of UreG, which is buried in the $UreG_2F_2H_2$ complex (29, 34, 39). Moreover, we have previously demonstrated that the nickel-charged UreG dimer can form a complex with $UreF_2H_2$ and apourease (20) and the interaction between UreG and $UreF_2H_2$ is essential to the urease activation (20, 24, 25). It is, therefore, likely that after receiving its nickel ion, the nickel-charged UreG dimer will dissociate from the $UreE_2G_2$ complex and activate urease by the formation of a complex with apourease and $UreF_2H_2$ (Fig. 6). It is currently not known how the nickel-charged UreG dimer interacts with apourease and $UreF_2H_2$ in the activation complex and what triggers the GTP hydrolysis during urease maturation. Presumably, premature GTP hydrolysis in the absence of $UreF_2H_2$/apourease would result in losing the nickel ion to the solution. As a result, GTP hydrolysis of UreG is likely triggered by the formation of the activation complex with $UreF_2H_2$ and apourease. It has been suggested that binding of $UreF_2H_2$ to urease can induce large conformational changes in urease (18, 19, 28), which may promote the recruitment of the nickel-charged UreG dimer from the $UreE_2G_2$ complex to the activation complex, where GTP hydrolysis is triggered for urease maturation (Fig. 6). Future structural studies on the activation complexes with apourease and urease accessory proteins such as UreG and $UreF_2H_2$ may help to fill in the knowledge gap here.

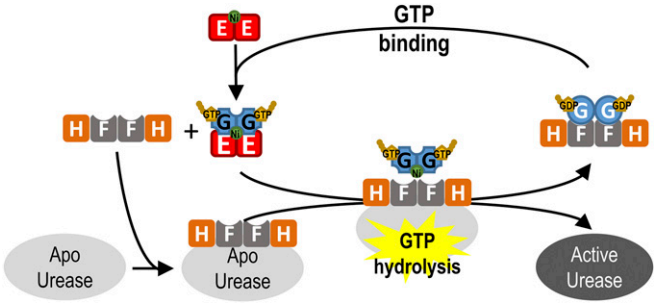

Fig. 6. How conformational changes in UreG during the GTP hydrolysis/binding cycle facilitate urease maturation. GTP binding induces conformational changes in UreG that destabilize the $UreG_2F_2H_2$ complex, causing UreG to dissociate from the complex and form the $UreE_2G_2$ complex with the nickel-charged UreE dimer. After receiving its nickel within the $UreE_2G_2$ complex, the nickel-charged UreG dimer is recruited to form the activation complex with apourease and $UreF_2H_2$. GTP hydrolysis induces conformational changes in the CPH motif of UreG, disrupting the square-planar coordination by Cys66/His68, and, hence, promotes release of the nickel ion for urease maturation. UreG, now in its GDP-bound state, prefers to form the $UreG_2F_2H_2$ complex, which is now ready to receive its nickel from $UreE_2$/Ni for another round of urease maturation.

Materials and Methods

Protein Expression and Purification. *H. pylori* apourease, $UreF_2H_2$ complex, and UreG and its mutant were expressed and purified as described previously (20, 24). *Kp*UreG was cloned into an in-house designed *pRSETA-His-SUMO* vector and expressed as an N-terminal HisSUMO-tagged fusion protein in *Escherichia coli*. The procedures for purification of *Hp*UreG were used to purify *Kp*UreG (20). Both *Hp*UreG and *Kp*UreG formed a stable dimer in the presence of Ni and GTP. The Ni/GTP-bound UreG dimers were prepared as described previously (20).

H. pylori UreE was cloned into pGEX-6p1 vector and expressed as an N-terminal GST-tagged fusion protein in *E. coli*. The transformed bacteria were grown to OD_{600} 0.5 and induced with 1 mM isopropyl beta-D-1-thiogalactopyranoside at 18 °C overnight. Cells were resuspended in 20 mM Hepes pH 7.5, 200 mM NaCl and 1 mM Tris(2-carboxyethyl)phosphine hydrochloride (TCEP) (buffer A) and lysed by sonication. After removal of cell debris by centrifugation at 20,000 × *g*, 60 min, the cell lysate was loaded onto a 5-mL GSTrap column (GE Healthcare) preequilibrated with buffer A. After extensive washing with buffer A, the GST-tagged UreE was eluted using 10 mM glutathione in buffer A. The GST-tag was cleaved using PreScission Protease (GE Healthcare) and the protein sample was dialyzed in 20 mM Tris pH 7.5, 50 mM NaCl and 1 mM TCEP (buffer B). The protein sample was loaded onto a 5-mL HiTrap-SP column (GE Healthcare) preequilibrated with buffer B, and UreE was eluted using 500 mM NaCl, 20 mM Tris pH 7.5 and 1 mM TCEP. To remove any bound metal in the UreE sample, 1 mM EDTA was added followed by gel filtration chromatography using a HiLoad Superdex 75 PG column (GE Healthcare) preequilibrated with buffer A.

Protein samples of nickel-charged UreE dimer were prepared by adding 1 mM $NiSO_4$ to 200 μM sample of UreE. Excess nickel in the protein sample was removed by a HiTrap Desalting column (GE Healthcare) preequilibrated with buffer A. To prepare the nickel-charged $UreE_2G_2$ complex, equal molar ratio (~100 μM) of nickel-charged UreE dimer and UreG was mixed in the presence of 2 mM $MgSO_4$ and 1 mM GTP, followed by gel filtration chromatography using a Superdex 200 Increase 10/300 gel filtration column (GE Healthcare). The amount of bound nickel in $UreE_2$ and $UreE_2G_2$ was estimated by atomic absorption spectroscopy (*SI Appendix*, Fig. S5). To prepare $UreE_2G_2$ complex without the bound nickel, apo-$UreE_2$ and UreG were mixed instead. The $UreG_2F_2H_2$ complex was prepared as described previously (20). The molecular weight of all protein samples prepared were analyzed by size-exclusion chromatography/static light-scattering (*SI Appendix*, Fig. S8).

Protein Crystallization and Structure Determination. Purified *Kp*UreG was dialyzed into 20 mM Tris buffer pH 7.5 containing 0.5 mM TCEP and concentrated to 14 mg/mL for crystallization. A total of 2 mM GMPPNP, 4 mM $MgSO_4$, and 2 mM $NiSO_4$ was added to the protein sample before crystallization. Full-length *Kp*UreG was crystallized but crystals were of poor diffraction quality. A truncated construct *Kp*UreG(ΔN4ΔC1) was used for crystallization to improve crystal quality. The protein was crystallized in 100 mM Hepes pH 7.5, 1.8 M $(NH_4)_2SO_4$, and 3% dioxane at 16 °C using the hanging-drop-vapor-diffusion setup. Crystals were cryoprotected by soaking

in a 1:1 mix of mother liquor with 3.4 M sodium malonate pH 7.0 solution, and flash frozen in liquid nitrogen. Diffraction data were collected using an in-house rotating anode X-ray generator (Rigaku FRE+) and a RAXIS IV imaging plate detector. Diffraction data were indexed and integrated using XDS (40) and scaled with AIMLESS (41) as programmed in Xia2 (42). Initial phases were determined by the molecular replacement method using the structure of *Hp*UreG found in the $UreG_2F_2H_2$ complex (PDB ID Code 4HI0) using the program PHENIX.AUTOMR (43). Initial models were build using PHENIX.AUTOBUILD and ARP/wARP (44) followed by iterative rounds of manual building using COOT (45) and refinement using PHENIX.REFINE (43). Correctness of the final models was checked using MOLPROBITY (46). To confirm the position of bound nickel in the crystals, diffraction data were also collected at the nickel peak wavelength using beamline I02 of the Diamond Light Source (*SI Appendix*, Fig. S1). For this dataset, the protein was crystallized in 100 mM Hepes pH 7.5, 1.8 M $(NH_4)_2SO_4$ and 4% ethylene glycol at 16 °C. The anomalous difference electron density was generated by PHENIX.REFINE. Figures of protein structures were created using PyMOL (www.pymol.org).

Size-Exclusion Chromatography/Static Light Scattering. SEC/SLS was used to obtain the elution profile and to estimate the molecular weight of protein complexes of urease accessory proteins. *H. pylori* urease accessory proteins were used in all SEC/SLS experiments. Protein samples were injected to a Superdex 200 Increase 10/300 gel filtration column (GE Healthcare) attached to a downstream miniDawn light scattering detector and an Optilab DSP refractometer (Wyatt Technologies), and preequilibrated with 20 mM Hepes pH 7.2, 100 mM NaCl, 0.2 mM TCEP (buffer C). Data were analyzed using the ASTRA software provided by the manufacturer.

For the studies of UreG dimerization (Fig. 3*A*) and UreE/UreG interaction (*SI Appendix*, Fig. S4), 100 μl of 30 μM protein samples (UreE and/or UreG) in 2 mM $MgSO_4$, 45 μM $NiSO_4$, and 300 μM GTPγS or GDP were mixed and incubated at room temperature for 10 min, before they were injected into the Superdex 200 Increase 10/300 column and analyzed by SEC/SLS. For the study of Ni/GTP-dependent dissociation of UreG from the $UreG_2F_2H_2$ complex (*SI Appendix*, Fig. S3), 100 μL of 15 μM of purified $UreG_2F_2H_2$ complex in 2 mM $MgSO_4$ and 300 μM GTPγS or GDP with 45 μM $NiSO_4$ were analyzed. For the study of effect of GTP hydrolysis on the urease accessory protein complexes (Fig. 4*A*), nickel-charged $UreE_2G_2$ complex and the $UreF_2H_2$ complex were mixed in equal molar ratio (~15 μM) and incubated at room temperature for 10 min before the protein samples were injected into the Superdex 200 Increase 10/300 gel filtration column with or without prior incubation of 10 mM potassium bicarbonate for 120 min at 37 °C. To test whether UreG or its mutant can swap protein-binding partners from $UreF_2H_2$ to $UreE_2$ upon GTP binding, (Fig. 4*B*), the $UreG_2F_2H_2$ complex and the nickel-charged UreE dimer were mixed in equal molar ratio (~15 μM) with or without 300 μM GTPγS and incubated at room temperature for 10 min before the protein samples were analyzed by SEC/SLS.

GTPase Assay. To investigate the effect of the *Hp*UreG mutant (D37A/E42A) on GTPase activity (Fig. 3*B*), 200 μL of 5 μM of *Hp*UreG (WT/mutant) was incubated in 2 mM $MgSO_4$, 300 μM GTP (or GTPγS), 10 mM potassium bicarbonate, 4 μM $NiSO_4$, 200 mM NaCl, 1 mM TCEP, 20 mM Hepes pH 7.5 buffer for 20, 40, and 60 min at 37 °C. Phosphate released was measured using a colorimetric assay based on malachite green as described (47).

In Vitro Urease Activation Assay. *H. pylori* urease accessory proteins and apourease were used for all in vitro urease activation assays. To investigate the effect of the UreG mutant (D37A/E42A) on urease activation (Fig. 3*C*), an in vitro urease activity assay using purified proteins was used. A total of 10 μM *H. pylori* apourease, 20 μM $UreF_2H_2$ complex, and 40 μM UreG (WT/mutant) were incubated in 20 mM Hepes pH 7.5, 200 mM NaCl, 1 mM TCEP, 2 mM $MgSO_4$, 10 mM potassium bicarbonate, 45 μM $NiSO_4$, and 300 μM GTP at 37 °C for 20 min. Urease activity was then determined by incubating the activated enzyme with 50 mM urea for 30 min at 37 °C and the ammonia released was measured using a phenol/hypochlorite reaction (48).

To investigate whether the nickel-charged UreE dimer, providing the sole source of nickel, can activate urease in vitro (Fig. 5*A*), 20 μM of nickel-charged UreE dimer was added to 10 μM of apourease with/without 20 μM of $UreG_2F_2H_2$ complex in the assay buffer (20 mM Hepes pH 7.5, 200 mM NaCl, 1 mM TCEP, 2 mM $MgSO_4$, 10 mM potassium bicarbonate, and 1 mM GTP). To investigate whether the nickel-charged $UreE_2G_2$ complex or nickel-charged UreG dimer can activate urease in vitro (Fig. 5 *B* and *C*), 20 μM of nickel-charged $UreE_2G_2$ complex or nickel-charged UreG dimer was added to 10 μM of apourease with/without 20 μM of $UreF_2H_2$ complex in the assay buffer. In all cases, activity of the activated urease was measured by the amount of ammonia released in 30 min at 37 °C using 50 mM urea as substrate (20).

To investigate whether protein–protein interactions are essential to the urease activation, urease accessory proteins ($UreE_2$/Ni, $UreG_2$/Ni, apo-$UreE_2$, apo-UreG, $UreG_2F_2H_2$, and $UreF_2H_2$) and apourease were added, as indicated in *SI Appendix*, Fig. S10, to either side of a dialysis membrane with a molecular weight cutoff of 6–8 kDa (Spectrum Labs) in a two-chamber dialyzer (Bioprobes, Ltd.). In the experiments reported in *SI Appendix*, Fig. S10*C*, 20 μM $NiSO_4$ was also added to the left chamber. The buffer in both chambers contained 20 mM Hepes pH 7.5, 200 mM NaCl, 1 mM TCEP, 2 mM $MgSO_4$, and 1 mM GTP. After equilibration at 4 °C for 16 h, 10 mM $KHCO_3$ was added to both chambers to activate the GTP hydrolysis required for urease activation. After incubation at 37 °C for 1 h, urease activity was determined as described above.

Circular Dichroism. Circular dichroism spectra of wild-type and D37A/E42A *Hp*UreG were measured with protein samples in 5 mM sodium phosphate buffer at pH 7.5 using a 0.5-mm path length cuvette with a JASCO J810 spectropolarimeter equipped with a Peltier-type temperature control unit.

ACKNOWLEDGMENTS. We thank Ms. Shu Nga Lui for her help in protein expression and purification and Dr. Yu-Wai Chen of King's College London and Dr. Pierre Aller of the Diamond Light Source for their help in diffraction data collection. This work was supported by grants from the Research Grants Council of Hong Kong (14117314 and AoE/M-05/12) and direct grants from The Chinese University of Hong Kong (3132814 and 3132815).

1. Andreini C, Bertini I, Cavallaro G, Holliday GL, Thornton JM (2008) Metal ions in biological catalysis: From enzyme databases to general principles. *J Biol Inorg Chem* 13: 1205–1218.
2. Waldron KJ, Rutherford JC, Ford D, Robinson NJ (2009) Metalloproteins and metal sensing. *Nature* 460:823–830.
3. Chandrangsu P, Rensing C, Helmann JD (2017) Metal homeostasis and resistance in bacteria. *Nat Rev Microbiol* 15:338–350.
4. Waldron KJ, Robinson NJ (2009) How do bacterial cells ensure that metalloproteins get the correct metal? *Nat Rev Microbiol* 7:25–35.
5. Foster AW, Osman D, Robinson NJ (2014) Metal preferences and metallation. *J Biol Chem* 289:28095–28103.
6. Macomber L, Hausinger RP (2011) Mechanisms of nickel toxicity in microorganisms. *Metallomics* 3:1153–1162.
7. Capdevila DA, Edmonds KA, Giedroc DP (2017) Metallochaperones and metalloregulation in bacteria. *Essays Biochem* 61:177–200.
8. Zeer-Wanklyn CJ, Zamble DB (2017) Microbial nickel: Cellular uptake and delivery to enzyme centers. *Curr Opin Chem Biol* 37:80–88.
9. Robinson NJ, Winge DR (2010) Copper metallochaperones. *Annu Rev Biochem* 79: 537–562.
10. Higgins KA, Carr CE, Maroney MJ (2012) Specific metal recognition in nickel trafficking. *Biochemistry* 51:7816–7832.
11. Pearson MA, Schaller RA, Michel LO, Karplus PA, Hausinger RP (1998) Chemical rescue of Klebsiella aerogenes urease variants lacking the carbamylated-lysine nickel ligand. *Biochemistry* 37:6214–6220.
12. Scott DR, Marcus EA, Weeks DL, Sachs G (2002) Mechanisms of acid resistance due to the urease system of Helicobacter pylori. *Gastroenterology* 123:187–195.
13. Farrugia MA, Macomber L, Hausinger RP (2013) Biosynthesis of the urease metallocenter. *J Biol Chem* 288:13178–13185.
14. Carter EL, Flugga N, Boer JL, Mulrooney SB, Hausinger RP (2009) Interplay of metal ions and urease. *Metallomics* 1:207–221.
15. Ge RG, Wang DX, Hao MC, Sun XS (2013) Nickel trafficking system responsible for urease maturation in Helicobacter pylori. *World J Gastroenterol* 19:8211–8218.
16. Kim JK, Mulrooney SB, Hausinger RP (2006) The UreEF fusion protein provides a soluble and functional form of the UreF urease accessory protein. *J Bacteriol* 188: 8413–8420.
17. Lee MH, Mulrooney SB, Renner MJ, Markowicz Y, Hausinger RP (1992) Klebsiella aerogenes urease gene cluster: Sequence of ureD and demonstration that four accessory genes (ureD, ureE, ureF, and ureG) are involved in nickel metallocenter biosynthesis. *J Bacteriol* 174:4324–4330.
18. Chang Z, Kuchar J, Hausinger RP (2004) Chemical cross-linking and mass spectrometric identification of sites of interaction for UreD, UreF, and urease. *J Biol Chem* 279: 15305–15313.
19. Farrugia MA, et al. (2013) Analysis of a soluble (UreD:UreF:UreG)2 accessory protein complex and its interactions with Klebsiella aerogenes urease by mass spectrometry. *J Am Soc Mass Spectrom* 24:1328–1337.
20. Fong YH, et al. (2013) Structure of UreG/UreF/UreH complex reveals how urease accessory proteins facilitate maturation of Helicobacter pylori urease. *PLoS Biol* 11: e1001678.

21. Boer JL, Quiroz-Valenzuela S, Anderson KL, Hausinger RP (2010) Mutagenesis of Klebsiella aerogenes UreG to probe nickel binding and interactions with other urease-related proteins. *Biochemistry* 49:5859–5869.
22. Carter EL, Hausinger RP (2010) Characterization of the Klebsiella aerogenes urease accessory protein UreD in fusion with the maltose binding protein. *J Bacteriol* 192: 2294–2304.
23. Soriano A, Hausinger RP (1999) GTP-dependent activation of urease apoprotein in complex with the UreD, UreF, and UreG accessory proteins. *Proc Natl Acad Sci USA* 96: 11140–11144.
24. Fong YH, et al. (2011) Assembly of preactivation complex for urease maturation in Helicobacter pylori: Crystal structure of UreF-UreH protein complex. *J Biol Chem* 286: 43241–43249.
25. Boer JL, Hausinger RP (2012) Klebsiella aerogenes UreF: Identification of the UreG binding site and role in enhancing the fidelity of urease activation. *Biochemistry* 51: 2298–2308.
26. Bange G, Sinning I (2013) SIMIBI twins in protein targeting and localization. *Nat Struct Mol Biol* 20:776–780.
27. Gasper R, Meyer S, Gotthardt K, Sirajuddin M, Wittinghofer A (2009) It takes two to tango: Regulation of G proteins by dimerization. *Nat Rev Mol Cell Biol* 10:423–429.
28. Quiroz-Valenzuela S, Sukuru SCK, Hausinger RP, Kuhn LA, Heller WT (2008) The structure of urease activation complexes examined by flexibility analysis, mutagenesis, and small-angle X-ray scattering. *Arch Biochem Biophys* 480:51–57.
29. Yang X, Li H, Lai TP, Sun H (2015) UreE-UreG complex facilitates nickel transfer and preactivates GTPase of UreG in Helicobacter pylori. *J Biol Chem* 290:12474–12485.
30. Wittinghofer A, Vetter IR (2011) Structure-function relationships of the G domain, a canonical switch motif. *Annu Rev Biochem* 80:943–971.
31. Kuppuraj G, Dudev M, Lim C (2009) Factors governing metal-ligand distances and coordination geometries of metal complexes. *J Phys Chem B* 113:2952–2960.
32. Yang X, et al. (2014) Nickel translocation between metallochaperones HypA and UreE in Helicobacter pylori. *Metallomics* 6:1731–1736.
33. Benoit SL, McMurry JL, Hill SA, Maier RJ (2012) Helicobacter pylori hydrogenase accessory protein HypA and urease accessory protein UreG compete with each other for UreE recognition. *Biochim Biophys Acta* 1820:1519–1525.
34. Bellucci M, Zambelli B, Musiani F, Turano P, Ciurli S (2009) Helicobacter pylori UreE, a urease accessory protein: Specific Ni(2+)- and Zn(2+)-binding properties and interaction with its cognate UreG. *Biochem J* 422:91–100.
35. Moncrief MBC, Hausinger RP (1996) Purification and activation properties of UreD-UreF-urease apoprotein complexes. *J Bacteriol* 178:5417–5421.
36. Farrugia MA, Wang B, Feig M, Hausinger RP (2015) Mutational and computational evidence that a nickel-transfer tunnel in UreD is used for activation of Klebsiella aerogenes urease. *Biochemistry* 54:6392–6401.
37. Zambelli B, et al. (2014) Nickel binding properties of Helicobacter pylori UreF, an accessory protein in the nickel-based activation of urease. *J Biol Inorg Chem* 19: 319–334.
38. Musiani F, et al. (2017) Protein tunnels: The case of urease accessory proteins. *J Chem Theory Comput* 13:2322–2331.
39. Merloni A, et al. (2014) Molecular landscape of the interaction between the urease accessory proteins UreE and UreG. *Biochim Biophys Acta* 1844:1662–1674.
40. Kabsch W (1988) Evaluation of single-crystal X-ray diffraction data from a position-sensitive detector. *J Appl Cryst* 21:916–924.
41. Winter G, Lobley CMC, Prince SM (2013) Decision making in xia2. *Acta Crystallogr D Biol Crystallogr* 69:1260–1273.
42. Winter G (2010) Xia2: An expert system for macromolecular crystallography data reduction. *J Appl Cryst* 43:186–190.
43. Adams PD, et al. (2010) PHENIX: A comprehensive Python-based system for macromolecular structure solution. *Acta Crystallogr D Biol Crystallogr* 66:213–221.
44. Langer G, Cohen SX, Lamzin VS, Perrakis A (2008) Automated macromolecular model building for X-ray crystallography using ARP/wARP version 7. *Nat Protoc* 3:1171–1179.
45. Emsley P, Lohkamp B, Scott WG, Cowtan K (2010) Features and development of coot. *Acta Crystallogr D Biol Crystallogr* 66:486–501.
46. Chen VB, et al. (2010) MolProbity: All-atom structure validation for macromolecular crystallography. *Acta Crystallogr D Biol Crystallogr* 66:12–21.
47. Baykov AA, Evtushenko OA, Avaeva SM (1988) A malachite green procedure for orthophosphate determination and its use in alkaline phosphatase-based enzyme immunoassay. *Anal Biochem* 171:266–270.
48. Weatherburn MW (1967) Phenol-hypochlorite reaction for determination of ammonia. *Anal Chem* 39:971–974.